All-or-none amyloid disassembly via chaperone-triggered fibril unzipping favors clearance of α-synuclein toxic species

Aitor Franco[a,b,1] , Pablo Gracia[c] , Adai Colom[a,b,f], José D. Camino [c], José Ángel Fernández-Higuero[a,b] , Natalia Orozco[a,b], Alexander Dulebo[d] , Leonor Saiz[e], Nunilo Cremades[c] , Jose M.G. Vilar[a,b,f], Adelina Prado[a,b] , and Arturo Muga[a,b,1]

[a]Biofisika Institute (CSIC, UPV/EHU), 48940 Leioa, Spain; [b]Department of Biochemistry and Molecular Biology, Faculty of Science and Technology, Campus Universitario, University of the Basque Country (UPV/EHU), 48940 Leioa, Spain; [c]Biocomputation and Complex Physics Institute (BIFI)-Joint Unit BIFI-IQFR (CSIC), University of Zaragoza, 50018 Zaragoza, Spain; [d]Bruker Nano Surfaces and Metrology Division, JPK BioAFM Business, 12489 Berlin, Germany; [e]Modeling of Biological Networks and Systems Therapeutics Laboratory, Department of Biomedical Engineering, University of California, Davis, CA 95616; and [f]IKERBASQUE, Basque Foundation for Science, 48013 Bilbao, Spain

α-synuclein aggregation is present in Parkinson's disease and other neuropathologies. Among the assemblies that populate the amyloid formation process, oligomers and short fibrils are the most cytotoxic. The human Hsc70-based disaggregase system can resolve α-synuclein fibrils, but its ability to target other toxic assemblies has not been studied. Here, we show that this chaperone system preferentially disaggregates toxic oligomers and short fibrils, while its activity against large, less toxic amyloids is severely impaired. Biochemical and kinetic characterization of the disassembly process reveals that this behavior is the result of an all-or-none abrupt solubilization of individual aggregates. High-speed atomic force microscopy explicitly shows that disassembly starts with the destabilization of the tips and rapidly progresses to completion through protofilament unzipping and depolymerization without accumulation of harmful oligomeric intermediates. Our data provide molecular insights into the selective processing of toxic amyloids, which is critical to identify potential therapeutic targets against increasingly prevalent neurodegenerative disorders.

neurodegeneration | α-synuclein | chaperone | disaggregase

Aberrant aggregation of α-synuclein (α-syn) into amyloid fibrils and subsequent accumulation into intracellular inclusions is a hallmark of neurodegenerative disorders such as Parkinson's disease, dementia with Lewy bodies, and multiple system atrophy (1–3). In these diseases, soluble α-syn monomers misfold and self-assemble, forming small oligomeric species that retain the highly disordered structure of the monomeric state (4). These species are rather unstable and can undergo structural rearrangements, including a gain in β-sheet structure that generates more stable species (4, 5). β-structured oligomers can grow further through monomer addition or self-association, finally giving rise to well-defined amyloid fibrils (4–6). Despite the controversial evidence about the relationship between the different species that populate the aggregation process and cellular toxicity, the prevalent view is that both intermediate oligomers and small fibrils are neurotoxic (7). Due to their abnormal interactions with cellular components, certain types of oligomers are key pathogenic agents in the development of the disease (8–10). In particular, they can disrupt membranes, induce oxidative stress, dysregulate calcium homeostasis, cause mitochondria dysfunction, or impair the proteasome system (11). Furthermore, α-syn oligomers have been implicated in the spreading of the disease, as these aggregates can be transmitted between cells (12, 13). Small fibrils have also been related to intercellular spreading and propagation of neurodegeneration (14–18). In contrast, large amyloid aggregates are believed to be relatively inert, as their highly ordered packing and slow diffusion reduces undesired interactions with cellular components. Even so, large aggregates can generate intermediate species that contribute to cytotoxicity through secondary processes such as fragmentation or nucleation on the aggregate surface (19, 20).

To counteract the toxic effect of protein aggregates, cells have evolved a sophisticated protein homeostasis network that coordinates protein synthesis, folding, disaggregation and degradation (21). This network is composed of the translational machinery, molecular chaperones and cochaperones, the ubiquitin-proteasome system, and the autophagy machinery. The way this network tackles amyloid aggregates remains poorly understood. It has been previously reported that the constitutive human Hsp70 (Hsc70) in collaboration with its Hsp40 cochaperone (Hdj1 or DnaJB1) slowly disassembles preformed α-syn fibrils (22). This activity was further stimulated by adding the NEF Hsp110 (Apg2). HspB5, a small heat shock protein also known as αB-crystallin, potentiated α-syn fibril disassembly by the ternary chaperone mixture. Although this chaperone combination was able to disaggregate fibrils, they did it in a timescale of weeks through a depolymerization process.

Significance

Although the human disaggregase machinery has been shown to disassemble mature α-synuclein amyloid fibrils, the molecular mechanism that drives the process has remained elusive. In this work, we show that amyloid disassembly is initiated by the destabilization of the fibril ends, followed by the fast propagation of protofilament unzipping and depolymerization along the fibril axis. This mechanism results in an all-or-none disaggregation of individual aggregates, avoiding the accumulation of harmful intermediate aggregated species. We specifically show that chaperones preferentially target the most toxic α-synuclein species, namely oligomers and short fibrils. Thus, our data provide a better understanding of the chaperone-mediated disaggregation at the molecular level, a crucial step to identify potential targets for the treatment of amyloid-related neurodegenerative diseases.

Only when Hsp104, a yeast representative of the Hsp100 family able of fragmenting fibrils, was added to the mixture, disassembly occurred within hours (22). The lack of Hsp104 homologs in metazoans questioned whether this activity was physiologically relevant in humans. A later study revealed that a chaperone complex composed solely of members of the Hsp70, Hsp40, and Hsp110 families was able to efficiently reverse α-syn amyloid fibrils through both fragmentation and depolymerization, generating smaller fibrils, oligomers, and, ultimately, monomers (23). Despite the importance of this emerging disaggregase functionality, its mechanism of action remains largely unknown. Recently, the same chaperone mixture has been reported to also disaggregate tau and Htt fibrils (24–26), pointing to this Hsp70-based machinery as a potential human amyloid disaggregase.

The two-fold aim of this work is, firstly, to test whether human disaggregase remodels with the same efficiency the different aggregates that populate the complex process of amyloid formation and, secondly, to shed light on the key mechanisms involved in the disassembly of amyloids. We show that the human disaggregase system disassembles toxic oligomers and short fibrils much better than large, less toxic fibrils, and that it does so by an enhanced destabilization of the small aggregated forms. Explicitly, fibril disassembly involves destabilization of the fibril ends and unzipping of the protofilaments, which allow depolymerization. The fast propagation of protofilament depolymerization toward the opposite fibril end is consistent with entropic pulling forces exerted by Hsc70 upon binding the fibril surface.

Results

Human Chaperones Disaggregate Toxic Oligomers of α-syn. Oligomeric assemblies formed during the early events of the amyloid self-assembly process accumulate in the brains and tissues of patients suffering from neurodegenerative disorders. These soluble oligomers are believed to be the primary origin of the toxicity in amyloid diseases (27). In this context, we wanted to explore the ability of the human disaggregase to process such toxic species. To this aim, we produced α-syn oligomers kinetically trapped during the self-assembly process, previously designated as type B* oligomers (4, 28, 29). The fluorescence resonance energy transfer signatures and biochemical behavior of these oligomers match those found for the transient oligomeric and toxic forms generated during aggregation (30, 31), although they are trapped under different conditions (32). Thus, they allow us to explore whether the disaggregase activity of chaperones can disassemble these aggregation intermediates found at the initial stage of the amyloid formation process. Endorsing previous studies (28, 29), these oligomers had a cylinder-like morphology and an average diameter of 10 to 40 nm, as seen by electron microscopy (EM) (Fig. 1A) and dynamic light scattering (DLS) (Fig. 1D). In terms of secondary structure, these oligomers have a β-sheet structure content intermediate between the intrinsically disordered monomers and the cross-β mature fibrils (*SI Appendix*, Fig. S1A) with a disordered N-terminal region and a highly hydrophobic solvent exposed β-sheet core. These two features have been proved to be key structural determinants for lipid membrane binding and disruption and, consequently, for their toxicity (28).

The presence of the Hsp40 component is essential for the disaggregase activity of the Hsp70 chaperone system. J-domain proteins (JDPs) form the largest chaperone family and guide Hsp70 to specific functions, therefore being responsible for the functional diversification of the central Hsp70 component (33). A recent report put forward a size-specific aggregate targeting for JDPs: large aggregates were preferentially targeted by a class B JDP, DnaJB1, whereas class A aimed for small ones (34). Being type B* oligomers small α-syn aggregates, we tested whether this specific targeting was also observed. To this aim, three different JDPs were assayed together with the Hsc70 and Apg2 components of the disaggregase: DnaJB1, a class B JDP involved in fibril disassembly (23), and two class A JDPs, DnaJA1 (Hdj2) and DnaJA2. Type B* oligomers of

α-syn were incubated with a five-fold excess of Hsc70 at an Hsc70:Hsp40:Apg2 molar ratio of 1:0.5:0.1, which gave maximum fibril disaggregation (*SI Appendix*, Fig. S1B) in agreement with previous data (23). Disaggregation reactions were directly resolved on a 4 to 16% Native-PAGE and analyzed by immunoblotting. The Hsc70-Apg2 combination showed disaggregase activity only with DnaJB1 and not with either of the class A JDPs (Fig. 1B). This activity was adenosine triphosphate (ATP)-dependent and resulted in the oligomeric to monomeric conversion of α-syn, with residual amounts of oligomeric species. These data indicate that Hsc70, working in concert with Apg2 and the same class B J-protein that disassembles fibrils, can target toxic oligomeric species formed at the early stages of the aggregation process.

Fibril Fragmentation Favors Chaperone-Induced Disaggregation. The overall aggregation process of α-syn, and other amyloidogenic polypeptides, was initially defined as a nucleation-polymerization process in which a primary nucleation step triggers oligomerization of the protein monomer (35). Later, it became evident that other secondary processes, such as nucleation catalyzed on aggregate surfaces and fibril fragmentation, also generated short fibrillar and toxic aggregation intermediates (19, 20, 36). In this regard, we also wanted to explore the effect of fibril fragmentation on the disassembly activity of the human disaggregase.

Mechanical fragmentation of fibrils by agitation or sonication produces a decrease in size and a concomitant increase in aggregate toxicity (37–41). Thus, to find out whether chaperone-induced fibril disassembly was size sensitive, we subjected α-syn fibrils to 15 or 30 sonication cycles and separated the soluble and insoluble fractions by centrifugation to obtain more homogeneous fibril populations (Fig. 1C). EM (Fig. 1C) and DLS (Fig. 1D) analysis of these samples confirmed that increasing sonication time consistently reduced fibril size. Importantly, as previously seen for other amyloid systems (37), sonication did not alter the conformation of α-syn fibrils, as infrared spectroscopy analysis of unsonicated and sonicated fibrils showed virtually identical spectra with absorption maxima at 1,628 cm^{-1} (*SI Appendix*, Fig. S1C), characteristic of proteins with cross-β structure (42). These different fibril preparations were incubated with chaperones to compare their disaggregation susceptibility, and the reaction products were analyzed by native electrophoresis to characterize the disassembly process. Regardless of the fibril size, fibril disassembly by the human disaggregase almost exclusively generated α-syn monomers (Fig. 1E) and its activity inversely correlated with fibril size (Fig. 1F), disaggregating shorter fibrils more efficiently.

The Human Disaggregase Disassembles Better the More Toxic α-syn Aggregates. We then sought to determine if there was a correlation between aggregate toxicity and chaperone targeting. One of the toxicity mechanisms described for α-syn is cellular membrane disruption (43), which can be mimicked in assays monitoring content release from liposomes (28). Addition of monomeric α-syn to liposomes produced negligible leakage of encapsulated calcein (Fig. 1G). Meanwhile, unsonicated fibrils provoked low content leakage—around 10%—and their fragmentation into shorter species increased proportionally their membrane-disrupting activity in a size-dependent manner, with the shortest fibrillar sample analyzed yielding similar membrane disruption as that induced by the oligomers (circa 45% maximum leakage). As previously observed (28, 29), content release from liposomes strongly correlated with the decrease in the viability of human neuroblastoma SH-SY5Y cells (Fig. 1H). At 0.3 μM α-syn, neither monomers nor unsonicated fibrils affected cell viability, but doubling the protein concentration reduced it by around 13% for both samples. As expected, we also observed an aggregate size–dependent reduction in cell viability upon addition of sonicated fibrils or type B* oligomers. The viability values obtained for the shortest fibrils and oligomers lowered to 75 and 66% at 0.3 and 0.6 μM α-syn, respectively, in agreement with
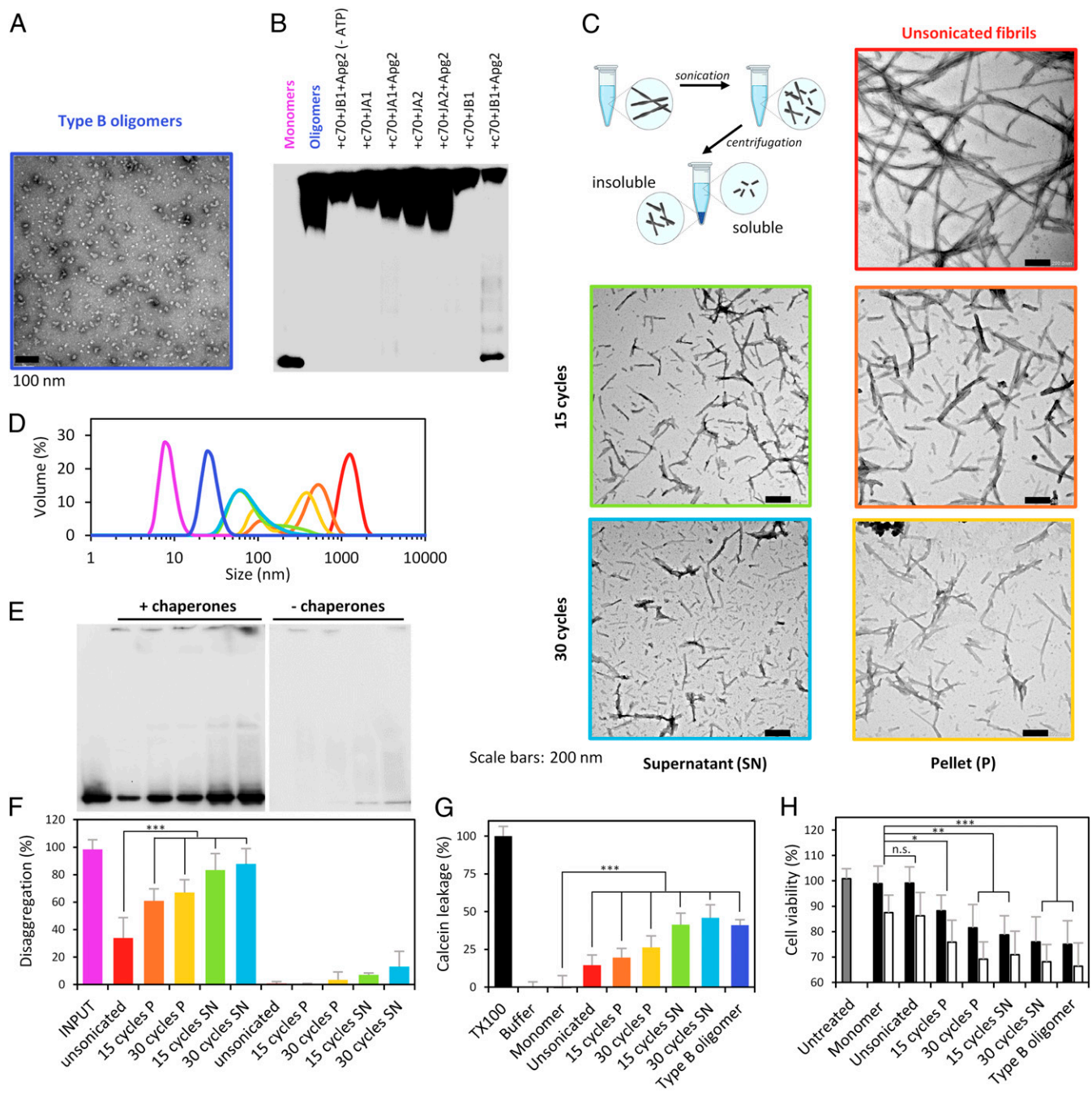
Fig. 1. The human disaggregase targets toxic aggregation intermediates of α-syn. α-syn type B* oligomers were visualized by TEM (*A*), and their disaggregation by different chaperone mixtures was analyzed by Native-PAGE and immunoblotting (*B*). Monomeric and oligomeric samples in the absence of chaperones were used as controls. (*C*) Schematic representation of the procedure used to obtain fibril populations of different sizes. Fibrils were either not sonicated (unsonicated) or sonicated using 15 or 30 cycles (1s ON, 1s OFF). After sonication, samples were centrifuged at 16,000 × *g* for 30 min to separate the soluble (SN) and insoluble (P) fractions and fibril size was analyzed by TEM. Size distribution of type B* oligomers and the different fibril populations was alternatively analyzed by DLS (*D*). Each sample is color-coded as shown in the previous panels. (*E*) 2 μM of α-syn fibrils of different lengths were incubated with 10 μM Hsc70, 5 μM DnaJB1, and 1 μM Apg2 in the presence of ATP and an ATP-regeneration system. Disaggregation reactions after 2 h incubation at 30 °C were analyzed by Native-PAGE and immunoblotting. The same concentration of monomeric (INPUT) and fibril samples in the absence of chaperones were used as controls. Disaggregation (%) was calculated as the amount of monomeric α-syn relative to the INPUT. Data are shown as mean ± SD of *n* = 4 independent experiments. (*G*) Membrane-disrupting activity of distinct α-syn aggregates. Liposomes with encapsulated calcein were incubated with different α-syn species (0.8 μM). Calcein release relative to the fluorescence signal obtained after LUVs solubilization using Triton X-100. Error bars, SD (*n* = 3). (*H*) Cell toxicity of different α-syn aggregates. Each aggregation state (0.3 or 0.6 μM α-syn) was added to SH-SY5Y cells, and after 24 h, incubation cell viability was measured monitoring mitochondrial activity by the reduction of MTS. Control cells in the absence of α-syn (untreated) are shown in gray. Error bars, SD (*n* = 5) (n.s.: not significant; *$P < 0.05$; **$P < 0.01$; ***$P < 0.001$).

Franco et al.
All-or-none amyloid disassembly via chaperone-triggered fibril unzipping favors clearance
of α-synuclein toxic species

PNAS | 3 of 11
https://doi.org/10.1073/pnas.2105548118
www.manaraa.com

previous reports (28). These data show that chaperones disassemble more efficiently the smaller β-sheet–rich aggregation intermediates of α-syn, which are the most toxic species.

Disassembly Kinetics of α-syn Aggregates Suggests an All-or-None Fast Solubilization Mechanism Favored by the Amyloid Structure. To get further insights into the mechanism used by chaperones to disaggregate α-syn amyloids, we monitored the disaggregation kinetics of fibrils and type B* oligomers using a fluorescence dequenching assay (4, 23). Alexa Fluor 488–labeled fibrils (unsonicated and sonicated) and type B* oligomers at 2 μM were mixed with different concentrations of the human disaggregase complex up to 1:2 α-syn:Hsc70 molar ratio. As we had previously characterized, the maximum disaggregation yield obtained for unsonicated fibrils at the highest chaperone concentration was around 15% (Fig. 2*A*). In stark contrast, sonicated fibrils (Fig. 2*E*) and type B* oligomers (Fig. 2*I*) were efficiently disaggregated in a dose-dependent manner, reaching maximum disassembly (85 to 100%) at 1:0.5 α-syn:Hsc70 molar ratio. Native-PAGE analysis of the disaggregation products of the three aggregate species showed that chaperone-mediated disassembly resulted in a major band corresponding to the monomeric protein (Fig. 2 *B*, *F*, and *J*), whose signal nicely paralleled the final disaggregation efficiencies calculated from fluorescence dequenching (*SI Appendix*, Fig. S2 *C and D*). Further confirmation that fluorescence dequenching assays represent the fibril disassembly reaction was obtained by an orthogonal assay using pyrene fluorescence excimer formation, a characteristic of the α-syn fibrillar state. For this, we used sonicated fibrils containing 20% pyrene-labeled α-syn (at position 85). The close proximity of pyrene molecules within the fibril allows formation of pyrene excimers with a characteristic fluorescence band at 470 nm, which is absent in the monomeric species (*SI Appendix*, Fig. S3) and is directly proportional to fibril concentration (32, 44). In the presence of the chaperone mixture, there was a decay in the fluorescence intensity of the pyrene excimer (*SI Appendix*, Fig. S3*A*) that overlapped the time dependence of the dequenching observed for Alexa Fluor 488–labeled sonicated fibrils (*SI Appendix*, Fig. S3*B*). The initial disassembly rates estimated by the disaggregation model (see *Materials and Methods*) were 0.038 and 0.039 min^{-1} for Alexa Fluor 488–labeled and pyrene-labeled sonicated fibrils.

Although some faint bands compatible with a very small fraction of low molecular weight oligomers were observed, the absence of larger intermediate species, especially under low disaggregation conditions (i.e., unsonicated fibrils at all chaperone concentration assayed or sonicated fibrils/type B* oligomers at low chaperone concentrations), suggested an all-or-none fast disassembly mechanism in which none or all of the monomers are extracted from each aggregate (seen on the top of the gels). To confirm that the main product of aggregate disassembly was monomeric α-syn from the beginning of the process, we analyzed the disaggregation of sonicated fibrils (*SI Appendix*, Fig. S4*A*) and type B* oligomers (*SI Appendix*, Fig. S4*C*) at different time points by Native-PAGE. Monomers represented the main band even at short times of the process. Bands corresponding to small oligomers were only detected when the gels were overexposed (*SI Appendix*, Fig. S4 *B and D*) and, importantly, their appearance did not precede monomer formation. In fact, monomeric and oligomeric bands appeared at the same time, although the concentration of oligomers was marginal with respect to that of the monomeric fraction. Interestingly, these minor oligomeric bands were also observed when chaperones were mixed with pure monomeric α-syn in the presence of ATP (*SI Appendix*, Fig. S4 *B and D*; INPUT [IP] lanes) and were not generated by α-syn–chaperone interactions (*SI Appendix*, Fig. S4*B*). Altogether, these data suggest that the minimal concentration of oligomers might arise from association events of monomeric α-syn after disassembly under the experimental conditions used.

This hypothesis was further supported by a mechanistic model that considers key parameters governing the disassembly reaction.

The model assumes a rate-limiting step for the transition from a chaperone-bound metastable state of the aggregate to its full disassembly. This type of process is characterized by a dwell time distribution of the metastable state described by an exponential decay (45). In the heterogeneous aggregate sample, there is a distribution of decay rates that was sensitive to the aggregation state (unsonicated or sonicated fibrils, oligomers) and the experimental conditions (substrate:chaperone molar ratio). Most of the aggregates were not susceptible to chaperone-induced disaggregation under the conditions tested in the case of unsonicated fibrils, whereas the opposite situation was obtained for sonicated fibrils and oligomers. The model analysis provides, as described in the *Materials and Methods* and *SI Appendix*, three key parameters: r_{max}, the maximum disaggregation rate; K_d, the apparent dissociation constant of the chaperone for the different aggregates; and n, a parameter indicating the cooperativity on the chaperone concentration. The model accurately described the time-dependent loss of aggregated α-syn at increasing chaperone concentrations (Fig. 2 *C*, *G*, and *K*). Comparison of the parameters inferred from the kinetics of the different aggregates (Fig. 2 *D*, *H*, and *L*) showed that the disaggregation rate of both types of fibrils reached saturation at about equimolar α-syn:Hsc70 concentrations, while it showed an almost linear dependence within the same chaperone concentration range for oligomers. This difference could be explained considering the lower affinity of chaperones for oligomers as compared with fibrils. Whereas the K_d values obtained for unsonicated and sonicated fibrils were similar (0.86 ± 0.06 and 0.84 ± 0.24 μM, respectively), the K_d estimated for oligomers was 11.53 ± 4.75 μM. The values of r_{max} inferred through the model showed that a major effect of fibril sonication is to induce a 30-fold increase in the maximum disaggregation rate and that this rate is substantially higher for oligomers than for fibrils. It is important to note that in the case of the oligomers, the disaggregation rate does not show any clear indication of saturation in the range of chaperone concentrations analyzed. Namely, the rate is largely proportional to the chaperone concentration with a proportionality coefficient given approximately by r_{max}/K_d. Therefore, only the ratio r_{max}/K_d is clearly identifiable (*SI Appendix*). To obtain a sensible estimation of K_d for oligomers, we had to constrain the cooperativity parameter to $n = 1$ based on the analysis of the unconstrained model (*SI Appendix*). Additionally, the cooperativity parameter around 1 obtained for sonicated fibrils ($n = 1.29 ± 0.29$) and oligomers ($n = 0.88 ± 0.20$) indicates that the disaggregation rate is essentially proportional to the binding of chaperones to the aggregate, and the value slightly lower than 3 for unsonicated fibrils ($n = 2.75 ± 0.44$) suggests that in the latter case, chaperone cooperation is needed for disaggregation to occur. The higher number of chaperone molecules required to trigger solubilization at much lower rates with the same affinity for chaperones suggests that although unsonicated fibrils are efficiently targeted by the chaperone system, they could be mechanically more stable than sonicated fibrils or oligomers, and therefore, it would be more difficult to engage them in a productive disassembly process.

Chaperone-Mediated Disaggregation of α-syn Fibrils Occurs through Fibril Unzipping and Depolymerization. To gain insights into the mechanism of chaperone-mediated fibril disassembly, we followed the disaggregation of unsonicated (*SI Appendix*, Fig. S5*A*) and sonicated (*SI Appendix*, Fig. S5*B*) α-syn fibrils with atomic force microscopy (AFM) under conditions that favor disaggregation, i.e., chaperone excess. Whereas mainly the smallest fibrils of the unsonicated sample were disassembled, most of the sonicated fibrils were disaggregated in a period of time that could not be properly resolved with conventional equipment. To follow such a fast process, we resorted to high-speed AFM. Sonicated fibrils were deposited on poly-L-ornithine coated mica and after an initial
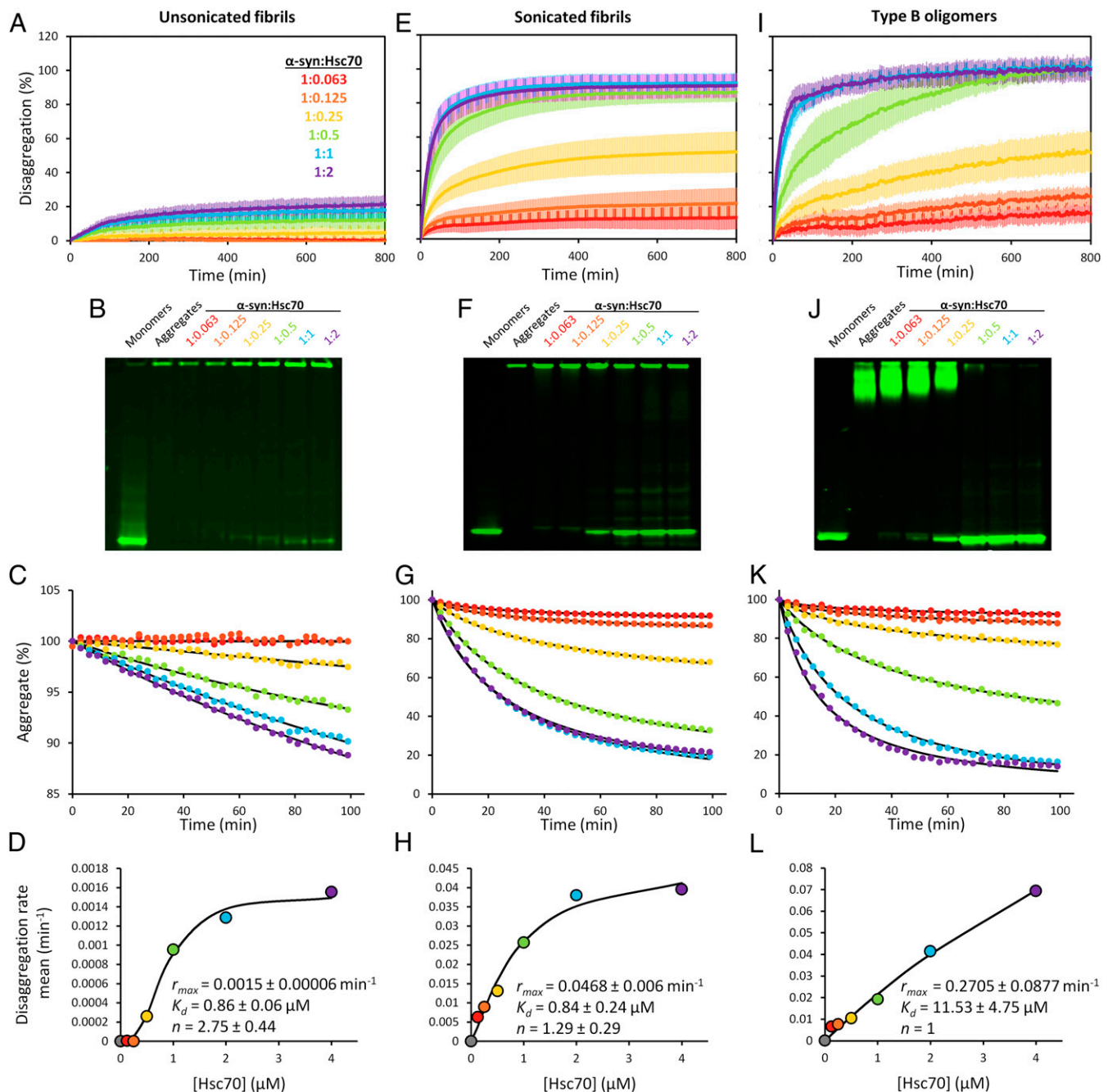
Fig. 2. Disaggregation kinetics of α-syn aggregates. Unsonicated α-syn fibrils (2 μM) (*A–D*), sonicated fibrils (*E–H*), and type B* oligomers (*I–L*) labeled with AlexaFluor488 were disaggregated at different chaperone concentrations with a molar ratio of Hsc70:DnaJB1:Apg2 constant at 1:0.5:0.1. Disaggregation was followed as a fluorescence dequenching process (*A*, *E*, *I*). Error bars represent SD ($5 < n < 10$). At the end of the kinetics, disassembly products were analyzed by Native-PAGE (*B*, *F*, *J*). The first 100 min (colored lines) from the aggregated mass time courses in (*A*, *E*, *I*) were fitted (black lines) to the aggregated mass decay expression (Eq. **1**) (*C*, *G*, *K*). The average disaggregation rates at each chaperone concentration were calculated from the inferred dynamic parameters (symbols) and the results fitted (lines) to a concentration dependent rate (Eq. **2**) (*D*, *H*, *L*). The values of the estimated parameters ± SD are given for each sample (*D* and *H*). In the case of type B* oligomers, the fit was constrained by setting $n = 1$ (*L*).

incubation to ensure the stability of the sample (*SI Appendix*, Fig. S5C and Videos S1 and S2), chaperones, ATP and an ATP-regeneration system were added to the chamber. Immediately after chaperone and nucleotide addition, fibril disaggregation events started to happen, with 42 events observed within the first 50 min (Fig. 3 *A*, *B*, and *D* and Video S3). No additional disassembly reactions were observed at longer incubation times (Fig. 3*D*), indicating that the time evolution of the disassembly events was in accordance with the fluorescence dequenching kinetics of similar

fibril samples (Fig. 2*E*). A second injection of the same chaperone and ATP concentrations promoted 10 more disaggregation events within 20 min (Fig. 3 *C* and *D* and Video S3).

Analysis of individual disaggregation events revealed the mechanism of the disassembly process. The time evolution of two representative disaggregation events are shown in Fig. 3 *E* and *F* and Videos S4 and S5. Interestingly, we observed that after destabilization of the fibril ends, unzipping of the protofilaments allows rapid depolymerization. In some events, chaperones

Franco et al.
All-or-none amyloid disassembly via chaperone-triggered fibril unzipping favors clearance of α-synuclein toxic species

destabilized and unzipped both fibrillar ends (Fig. 3*E* and Video S5), indicating that fibril depolymerization could start at any or both of the two fibril tips. Yet, the fast propagation of the disassembly process favored unidirectional disaggregation in most cases (Videos S6–S8). This mechanism would favor disaggregation of short, toxic fibril species, as the number of fibril tips
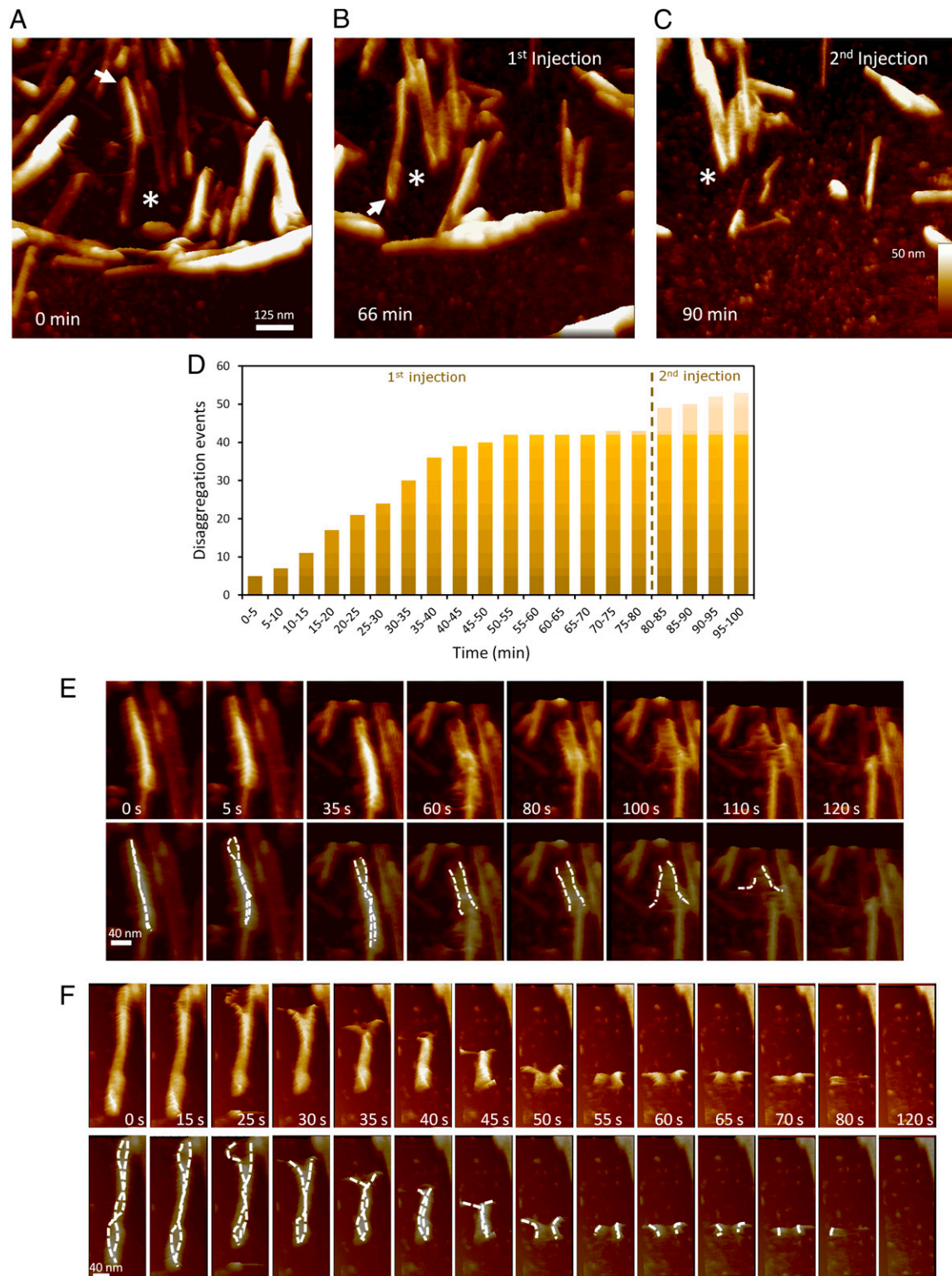

Fig. 3. Chaperone-mediated disaggregation of α-syn fibrils followed by high-speed AFM. High-speed AFM movie frames of the chaperone-mediated disaggregation of α-syn sonicated fibrils immediately after addition (time 0) of chaperones, ATP, and an ATP-regeneration system to the chamber (*A*) and after 66 min incubation (*B*). At 80 min, a second injection of chaperones and nucleotide was done, further scanning until 90 min (*C*). White asterisks in *A*–*C* represent the same scan location, which drifted during the measurement. (*D*) Cumulative disaggregation events were plotted as a function of time. (*E* and *F*) Time-resolved disassembly of individual fibrils marked with white arrows in *A* (*E*) and *B* (*F*).

All-or-none amyloid disassembly via chaperone-triggered fibril unzipping favors clearance

available is considerably higher than for unsonicated ones. In the case of large, unsonicated fibrils, lateral interfibril association might also impair the depolymerization reaction as it could decrease binding of Hsc70 molecules to these regions and/or negatively affect the unzipping mechanism.

The Aggregate-Size Dependence Disassembly Activity of the Human Disaggregase Is Conserved for Tau Fibrils. To test whether the aggregate-size dependence described for α-syn fibrils also occurred for other amyloidogenic proteins, we assembled tau fibrils from the recombinant full-length isoform 2N4R (Fig. 4*A*) and fragmented them by sonication, which leads to the formation of smaller toxic species (38). The unsonicated and sonicated fibrillar samples were treated with the human disaggregase and their solubilization was analyzed by a sedimentation assay. Chaperones solubilized poorly (around 6%) unsonicated tau fibrils, while disaggregation increased substantially (up to 42%) for the sonicated sample (Fig. 4*C*). These findings suggest that the preferential targeting of smaller aggregation intermediates by the human disaggregase might apply to other amyloidogenic proteins.

Discussion

The human Hsp70-based chaperone system has been shown to revert α-syn fibrils, although the exact disaggregation mechanism has remained unclear despite the two proposed models (22, 23). Both models propound that human disaggregase depolymerizes fibrils extracting monomers from their ends, whereas one of them also puts forward that chaperones can extract monomers from the center of the fibrils, therefore breaking them into smaller fragments (23). We show that long, unsonicated α-syn fibrils are poorly disassembled by chaperones unless they are mechanically fragmented through sonication, which increases the number of fibril ends and reduces their lateral association and most likely the pulling force necessary to unzip the protofilaments. Disassembly of sonicated fibrils yields monomeric α-syn without the accumulation of a significant concentration of aggregation intermediates. Indeed, we show that this chaperone machinery can also efficiently disaggregate small toxic oligomeric species of α-syn with the same class B JDP, DnaJB1.

The lack of a representative amount of aggregation intermediates indicates that disaggregation takes place as an all-or-none phenomenon (46, 47) at the aggregate level, meaning that individual aggregates are not processed in a slow and gradual manner following the macroscopic disaggregation kinetics but rather through an abrupt and fast asynchronous process. Kinetic analysis of the fluorescence dequenching time courses showed that solubilization data are consistent with this observation and high-speed AFM analysis demonstrates indeed that is the case for fibrils. In this regard, the solubilization of amyloids cannot be interpreted in terms of a population of aggregates with decreasing size over time. Instead, it should be interpreted as a population with decreasing number of aggregates over time. This change of paradigm in the disaggregation process would be consistent with our current view of aggregate toxicity, in which smaller aggregates are associated with higher toxicity. The human disaggregase system eliminates them one by one rather than increasing the toxicity of the aggregates by progressively reducing their size.

A finding that deserves discussion is the fast propagation of disassembly in individual fibrils, considering that the highly organized structure of amyloids is the most stable aggregate state from a thermodynamic point of view. Yet, the fibrillar structure of amyloids allows Hsc70 to interact throughout the whole aggregate surface (23), binding up to every other protomer in the case of α-syn fibrils (48). This α-syn to Hsc70 stoichiometry (1:0.5) is consistent with our disaggregation experiments, which would yield a similar molar ratio under saturation conditions. The disaggregation model suggests that the affinity of Hsc70 for α-syn fibrils does not depend on their length,
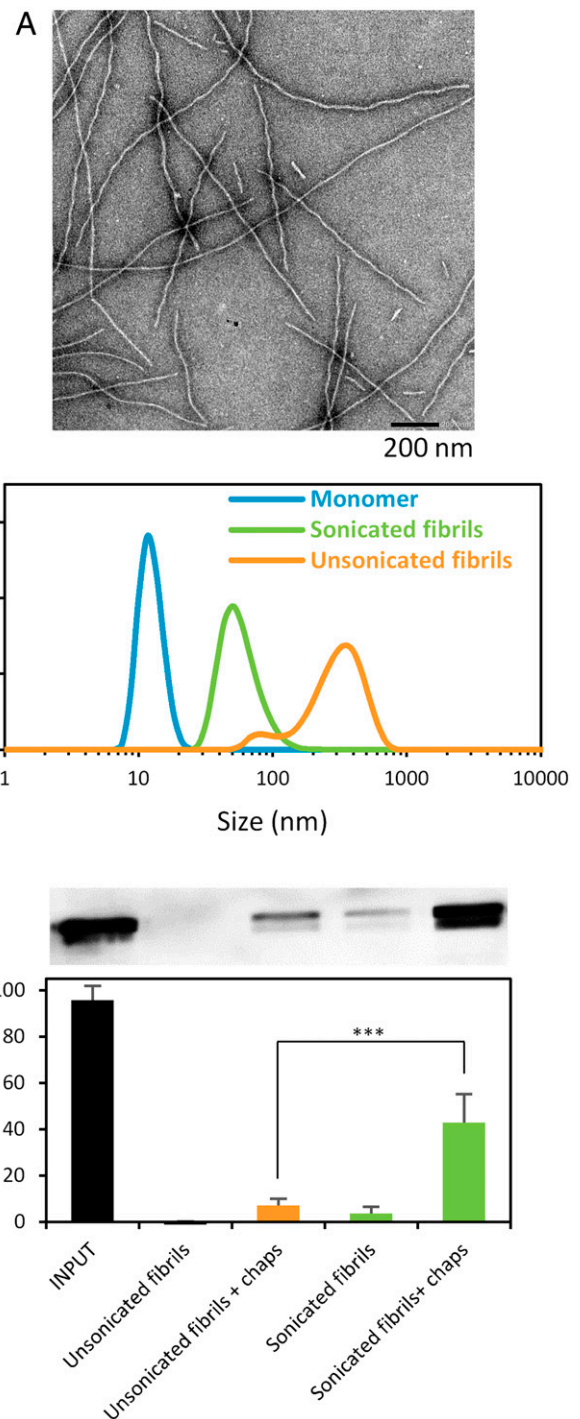

Fig. 4. Fragmentation of Tau fibrils allows chaperone-mediated disaggregation. (*A*) TEM of tau 2N4R fibrils. (*B*) DLS-derived size distribution of monomeric and fibrillar (unsonicated and sonicated) tau samples. (*C*) Solubilization of tau fibrils (1 μM) by the human disaggregase was analyzed by a sedimentation assay. After 2 h incubation at 30 °C, reaction mixtures were centrifuged, and solubilized tau in the supernatant was detected by immunoblotting. Fibrils without chaperones were used as a control. INPUT was made with a 1-μM solution of monomeric tau. Error bars represent SD for $n = 4$ independent experiments (***$P < 0.001$).

as expected if the structure and accessibility of the chaperone binding sites do not change with fibril size. However, the number of binding sites available for the chaperone could be reduced in the unsonicated fibrils due to interfibril assembly, therefore resulting in a weaker

BIOPHYSICS AND COMPUTATIONAL BIOLOGY

pulling force at the aggregate surface than that required for unzipping and disassembly. A change in the structure and/or accessibility of the chaperone binding sites in the oligomer could explain the loss of chaperone affinity for this aggregation intermediate. The different types of β-sheet structure reported for type B* oligomers (antiparallel) and fibrils (parallel) also indicates that the human disaggregase can remodel both assemblies regardless of the conformation of their structural cores (11, 32). The lower number of residues involved in the cross β-structure and resistance to proteinase K degradation observed for these oligomers as compared with fibrils (29), reflects a reduced stability of the oligomeric assembly that could explain, at least in part, its faster disaggregation rate. Moreover, if as a consequence of the disaggregase activity of the chaperone mixture, the number of monomers within the oligomers is reduced from 25 to 30 to around 10, the oligomeric structure is expected to become unstable enough to spontaneously disassemble into monomers (29). This implies that the chaperone action would be required only during the initial step of the disassembly reaction, since when the size of the oligomer is small enough, it could dissociate regardless of chaperone activity (11, 29). This might also help to explain the higher disaggregation rates obtained for oligomers, as compared with fibrils, considering the lower affinity of the chaperone for these type of oligomers.

The DnaJB1-induced increase in the affinity of Hsc70 for the amyloid substrate provides the energy required to load the chaperone in this dense arrangement (48). Crowding of Hsc70 at the fibril surface provokes steric clashes between neighboring Hsc70 molecules, an energetically unfavorable situation that exerts entropic pulling forces on Hsc70-bound α-syn molecules (48). Furthermore, the high molecular mass of Apg2 could impede the shuffling of crowded Hsc70 molecules, biasing NEF activity to those chaperone molecules that are not densely packed on the fibrils (48). Therefore, we rationalize that Apg2 preferentially interact with the fibril ends or nearby regions, where the excluded volume effect of Hsc70 molecules is the lowest, explaining why fibril unzipping and depolymerization starts at this location (Fig. 5). Time-resolved AFM clearly shows that depolymerization starts by fibril unzipping at the fibril tips and propagates fast through the fibril axis. Fast propagation could be due to the unfavorable dense

packing of Hsc70 molecules along the protofilaments, which would destabilize them exerting the pulling force required to extract monomers as Hsc70 molecules become accessible to Apg2 due to progressive depolymerization. The "ram´s horns" motif observed during depolymerization suggests unzipping of the twisted filaments that build the fibril, which could be necessary for monomer extraction (Fig. 5).

Fibril fragmentation by sonication increases the number of ends and reduces interfibril interactions, i.e., fibril clumping, and thus, it might enhance the likelihood of starting a depolymerization process. Within α-syn fibrils, each monomer establishes intra- and interprotofilament interactions with neighboring monomers (49–57). Monomers located at the end of the fibril lack half of these interactions and thus, their extraction is energetically less demanding. This, together with the fact that Apg2 could be sterically excluded from the fibril center due to Hsc70 crowding (48), lead us to the conclusion that fibril fragmentation by chaperones may not be favorable. Nonetheless, a previous report showed fibril shortening within a few minutes after chaperone addition that was attributed to fragmentation (23). Our results suggest that this observation is compatible with a fast depolymerization-only mechanism that could be eventually interrupted in large fibrils (i.e., unsonicated sample). Fibril clumping, which is observed to a greater extent in unsonicated fibrils, likely contributes with an additional energetic penalty to protofilament unzipping and therefore to disaggregation. Another factor that might also hinder disaggregation could be the length of the fibril. The longest the fibril, the more interactions between the twisted protofilaments that contribute to its stabilization, with the expected increase in the energetic demand for remodeling. These factors could slow down the unzipping process or halt it before it reaches the opposite fibril end, rendering monomers and shorter fibrils without altering the number of fibril ends. The lack of fragmentation observed when the same chaperone complex acts on tau fibrils (24) further supports this hypothesis, which is also corroborated with our results showing that chaperone activity was only significant after mechanical fragmentation of tau fibrils.

An important aspect to decipher the consequences of the Hsp70-based amyloid disassembly activity in neurodegeneration
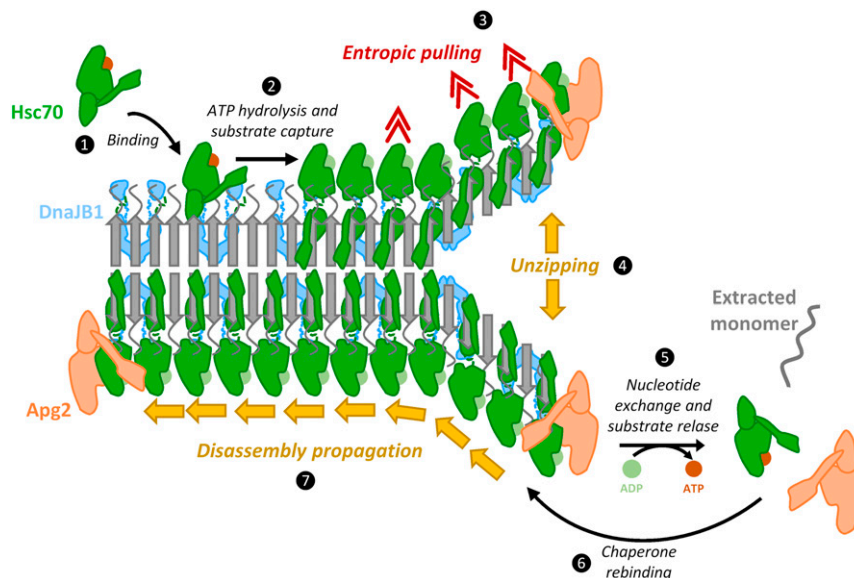

Fig. 5. Model proposed for the disassembly of α-syn fibrils by the human disaggregase. DnaJB1 recruits Hsc70 to the fibril surface, where it can reach a binding stoichiometry of 1:0.5 (α-syn:Hsc70). The high Hsc70 density on the fibril surface induces an exclusion volume effect on Apg2, a necessary factor for fibril disassembly, which is displaced to the fibril ends to interact with the chaperone. Destabilization of the tips as a consequence of the joint chaperone action is followed by fast protofilament unzipping and monomer extraction, which could be facilitated by the entropic pulling forces generated by Hsc70 crowding that facilitate complete disaggregation.

is to consider the toxicity of the disaggregation products. The initial in vitro observations indicated that α-syn disaggregation could be beneficial and cytoprotective since fibrillar α-syn was eventually dissolved into less toxic species (23). Furthermore, altering the human disaggregase activity can have beneficial effects on α-syn aggregation in cell culture and animal models (58, 59). Our data suggest that this beneficial effect is expected as the human disaggregase efficiently solubilizes toxic α-syn oligomers into monomers. Nevertheless, it has also been reported that the chaperone-mediated disaggregation process could also generate spreading-competent oligomeric and short fibrillar species that may serve as a template for further aggregation (24, 59). As pointed out by Tittelmeier et al. (59), the Hsp70-based disaggregation activity could be a double-edged sword as it is essential in maintaining proteostasis but could also generate toxic amyloid species. The final outcome might depend on the state of the protein quality control network, which declines with aging and disease. The high proteostasis capacity characteristic of healthy or young organisms could ensure fast disaggregation of toxic amyloids, including oligomers and small fibrils, reducing their lifetime and thus, their negative intracellular and spreading effects. The high Hsc70 concentration in human cells, estimated to be around 10 μM (60), would facilitate aggregate disassembly even at cellular locations where the concentration of α-syn could be higher (μM range) (61) than average (nM range) (62). In the extracellular medium, disassembly of α-syn aggregates involved in cell-to-cell disease spreading might be compromised by the low concentration of α-syn and Hsc70, which in both cases has been estimated to be in the low nM range (63, 64), and the availability of cofactors. Therefore, our data are consistent with a disaggregase action of the Hsc70 system provided that chaperone concentration involved in this task is high enough, but do not ensure that in the extracellular medium the disaggregase would be active. In contrast, in sick or old individuals the proteostasis capacity gets progressively impaired due to a reduction in the chaperones available to process toxic aggregates, which transiently accumulate, inducing cell-death and spreading from cell to cell (65).

Materials and Methods

Protein Overexpression and Purification. Chaperones were produced as previously reported (66). α-syn and tau 2N4R, cloned in pT7-7 and pRK-T42 vectors, were expressed in *E. coli* BL21 (DE3) cells. α-syn was purified from the periplasm by performing an osmotic shock followed by an anion exchange chromatography as described previously (67). The cysteine-containing α-syn mutants were expressed and purified as the WT protein but including 2 mM DTT in all purification steps. Tau 2N4R was purified according to ref. 68.

Labeling of Proteins. Alexa Fluor 488–labeled Q24C α-syn and pyrene-labeled A85C α-syn were obtained following the protocol previously described to label cysteine-containing variants with maleimide-derivatized fluorophores (32). Labeling efficiency (85 to 100%) was estimated spectrophotometrically, using $\varepsilon_{494} = 72,000\ M^{-1} \cdot cm^{-1}$ for Alexa Fluor 488, $\varepsilon_{344} = 22,000\ M^{-1} \cdot cm^{-1}$ for pyrene, and $\varepsilon_{280} = 5,960\ M^{-1} \cdot cm^{-1}$ for protein concentration, after subtracting the contribution of the absorption of the dye at the respective wavelengths.

α-syn Aggregates Preparation. α-syn type B* oligomers, which have been related to the toxic transient oligomeric species formed during fibril formation (32), were obtained by lyophilization as previously described (29). This experimental procedure gave reproducible oligomer populations with size distribution of 10 to 40 nm, as reported (*SI Appendix*, Fig. S2A) (29). To prepare α-syn fibrils, a 100-μM protein solution was incubated at 37 °C under orbital agitation (1,000 rpm) for 7 d in 50 mM Tris, 100 mM NaCl, and 0.05% NaN₃, pH 7.4. Afterward, fibrils were purified by centrifugation for 30 min at 16,000 × g and 4 °C. Pelleted fibrils were resuspended, unless otherwise stated, in Disaggregation Buffer (40 mM Hepes-KOH pH 7.6, 50 mM KCl, 5 mM MgCl₂, and 2 mM DTT). Aggregates labeled with fluorescent dyes contained 8 to 20% labeled α-syn molecules, a concentration range that did not significantly affect the kinetics of the chaperone-mediated disassembly reaction. The final protein concentration (monomer equivalents) was determined by disassembling an aliquot of the preparation into monomers in 4 M GdnHCl and measuring its absorption at 280 nm. Sonicated fibrils were

obtained using a Branson 450 Digital Sonifier equipped with a tapered microtip of 3 mm diameter at 10% power. Bursting was carried out in cycles of 1 s ON, 1 s OFF with the sample set on ice-cold water. To obtain α-syn fibrils of different sizes, soluble and insoluble fractions of samples sonicated for 15 or 30 cycles were separated by centrifugation (30 min at 16,000 × g and 4 °C). Pellets were resuspended in Disaggregation Buffer and supernatants were passed through 100 K AmiconUltra 0.5-mL filters to remove any possible monomer released during sonication. This procedure consisted of seven washing steps (4 min at 10,000 × g and 20 °C) with 400 μL of Disaggregation Buffer. For the kinetic analysis, sonicated fibril samples were obtained after a total of 90 sonication cycles. This protocol yielded reproducible samples with a size distribution in the 30 to 200 nm range and centered at around 90 nm as seen by DLS (*SI Appendix*, Fig. S2A) and EM (*SI Appendix*, Fig. S2B). When labeled fibrils were prepared, a monomeric α-syn solution that contained 15 to 20% of Alexa Fluor 488–labeled α-syn_Q24C or pyrene-labeled α-syn_A85C was seeded with 5% (mol/mol) of preformed sonicated fibrils and incubated at 37 °C under quiescent conditions for 1 to 4 d. Labeled fibrils were purified as explained. Labeled type B* oligomers were prepared as unlabeled ones but with 25% of Alexa Fluor 488–labeled α-syn_Q24C.

Tau Fibrils Preparation. Tau 2N4R fibrils were prepared at 40 μM tau 2N4R in the presence of 40 μM heparin (MW 3,000, MPBio) in 25 mM Tris pH 7.5, 50 mM NaCl, and 2 mM DTT supplemented with 1 mM PMSF, 1 mM EDTA, 1 mM EGTA, 1 μg/mL leupeptin, 1 μg/mL aprotinin, 1 μg/mL pepstatin, and 0.05% NaN₃. Samples were incubated at 37 °C under quiescent conditions for 7 d, refreshing the DTT every day. Sonicated fibrils were obtained by 15 sonication cycles (1 s ON, 1 s OFF). Monomer-free unsonicated and sonicated fibrils were obtained by ultracentrifugation for 40 min at 186,000 × g and 4 °C and resuspension in Disaggregation Buffer.

DLS. Size volume distribution profiles of the different samples at 25 °C were obtained using a Zetasizer Nano ZS (Malvern Instruments) at a back scattering angle of 173°. Monomeric (100 μM) and oligomeric or fibrillar (10 μM) α-syn and tau species were measured in Disaggregation Buffer.

Circular Dichroism. Far-UV CD spectra of samples containing 10 μM α-syn in PBS were acquired at 20 °C in a Jasco J-810 circular dichroism spectropolarimeter using rectangular quartz cuvettes with 1 mm path length. Each spectrum represents the average of 15 to 20 scans, collected from 200 to 260 nm, with a spectral bandwidth of 1 nm and a response time of 1 s.

FT-IR Spectroscopy. Aggregates (1 to 10 mg/mL) were exchanged into deuterated PBS buffer and applied on a 25-μm carved calcium fluoride window mounted in a Peltier cell (TempCon, Bio Tools). Spectra were collected with a nominal resolution of 2 cm⁻¹ in a Nicolet Nexus 5700 spectrometer equipped with a MCT detector at 20 °C. They were digitally subtracted using a spectrum of deuterated buffer as a reference, and the area of the amide I band (1,700 to 1,600 cm⁻¹) was normalized in all spectra (42).

EM. The 3 μL samples (1 to 2 mg/mL) were applied onto glow-discharged Formvar/carbon-coated 200-mesh copper grids and incubated for 1 min. Grids were negatively stained with 1% (wt/vol) uranyl acetate (two staining steps of 10 s) and air-dried for 5 min. Samples were visualized in a JEOL JEM 1400 Plus electron microscope.

PAGE-Based Chaperone-Mediated Disaggregation. The 2 μM α-syn fibrils were incubated with 10 μM Hsc70, 5 μM DnaJB1, and 1 μM Apg2 in Disaggregation buffer supplemented with 2 mM ATP and ATP-regeneration system (8 mM PEP, 20 ng/μL pyruvate kinase). After 2 h incubation at 30 °C, samples were centrifuged for 30 min at 16,000 × g and 4 °C, and supernatants were carefully collected, mixed with SDS-containing loading buffer, boiled for 10 min, and analyzed by SDS-PAGE and immunoblotting using an anti–α-syn antibody (Invitrogen PA5-85343, 1:2,000 dilution). Hsc70 and Apg2 were detected by using the monoclonal antibodies Abcam ab51052 and Abcam ab185962, respectively, at 1:5,000. Alternatively, after the incubation at 30 °C, samples were directly run in a Native-PAGE 4 to 16% Bis-Tris gels (Invitrogen) and analyzed by immunoblotting. Tau 2N4R disaggregation was followed by a sedimentation assay similar to that described for α-syn with the following changes: samples contained 1 μM tau, 10 μM Hsc70, 5 μM DnaJB1, and 1 μM Apg2, and after the 2 h incubation at 30 °C, they were centrifuged for 40 min at 186,000 × g and 4 °C. For tau detection, a polyclonal antibody (Dako A0024, 1:50,000 dilution) was employed.

Franco et al.
All-or-none amyloid disassembly via chaperone-triggered fibril unzipping favors clearance of α-synuclein toxic species

PNAS | 9 of 11
https://doi.org/10.1073/pnas.2105548118

www.manaraa.com

Disaggregation Kinetics. Disaggregation was carried out in 96-Well Half Area Black plates (Nonbinding surface; Corning) at a final α-syn concentration of 2 μM. Then, 20 μL of aggregates were mixed with 25 μL of increasing chaperone concentrations. No disaggregation (0%) and complete (100%) disaggregation controls were obtained with aggregates alone or monomers in the presence of chaperones, respectively. Before starting the reaction, samples were stabilized for 30 min at 30 °C in the plate reader. The reaction was initiated with the addition of 5 μL of a mixture of ATP and ATP-regeneration system, and afterward, plates were sealed with HD Clear duct tape and measured. Fluorescence readings were collected every 3 min from the top, using excitation and emission filters of 485/20 and 528/20 nm and a gain of 60 to 75. Quenching was greater for fibrils than for type B* oligomers, and therefore the difference in fluorescence signal between the aggregates and the monomer was larger in the case of the fibrils. At the end of the kinetics, samples were analyzed by Native-PAGE and in-gel fluorescence was visualized in a VersadocMP. Only the monomeric band was used to quantify fibril disassembly, and the intensity of a band corresponding to the same protein mass concentration of a pure monomeric protein sample was considered 100% disaggregation. For pyrene-labeled fibrils, fluorescence was monitored using excitation and emission wavelengthsat 337 nm and 470 nm, respectively, under the same experimental conditions.

Disaggregation Modeling. We considered disaggregation as an activated process that leads to the sudden solubilization of aggregates into monomers (*SI Appendix*). The survival probability P_a of an aggregate a follows an exponential decay $P_a(t) = e^{-k_a t}$ with rate k_a. The expected total aggregated mass as a function of time for an ensemble of aggregates with individual masses m_a follows from $m(t) = \sum_a m_a P_a(t) = \sum_a m_a e^{-k_a t}$, which results in a disaggregation kinetics $\frac{dm(t)}{dt} = -r(t)m(t)$ with a time-dependent disaggregation rate $r(t) = \frac{\sum_a k_a m_a e^{-k_a t}}{\sum_a m_a e^{-k_a t}}$. We characterized the overall aggregate heterogeneity as $\sum_a m_a e^{-k_a t} = m(0) \int f_{\alpha,\beta}(k_a) e^{-k_a t} dk_a$, where $f_{\alpha,\beta}(k_a) = \frac{\beta^\alpha}{\Gamma(\alpha)} k_a^{\alpha-1} e^{-\beta k_a}$ is a gamma distribution with shape α and rate β. This characterization leads to an overall aggregated mass decay,

$$m(t) = \frac{m(0)}{\left(1 + \frac{t}{\beta}\right)^\alpha}, \qquad [1]$$

that closely mimics the observed kinetics of disaggregation. The disaggregation rate in terms of these parameters is given explicitly by $r(t) = \frac{\alpha}{\beta}\left(1 + \frac{t}{\beta}\right)^{-1}$, which at time 0 provides the average disaggregation rate as $r(0) = \frac{\sum_a k_a m_a}{\sum_a m_a} = \frac{\alpha}{\beta}$.

To characterize this rate under different conditions, we obtained the parameters α and β for each case by fitting the expected dynamics to fluorescence dequenching time courses over the first 100 min of the disaggregation process. To investigate the effects of the chaperone concentration [c] on the resulting average disaggregation rates, we subsequently fitted the results to a concentration-dependent rate with a functional form

$$r(0) = r_{max} \frac{([c]/K_d)^n}{1 + ([c]/K_d)^n}, \qquad [2]$$

where n is a cooperativity parameter; K_d is the apparent dissociation constant of the chaperone to the aggregate; and r_{max} is the saturation rate.

Calcein Leakage. To prepare liposomes with encapsulated calcein, 4 mg of POPS, dissolved in chloroform:methanol (2:1) at 25 mg/mL, were dried and swollen in Encapsulation Buffer (10 mM Hepes-KOH, 50 mM NaCl, and 50 mM

calcein, pH 7.4) with two cycles of heating to 50 °C and vortexing. The multilamellar vesicles (MLVs) obtained were used to generate large unilamellar vesicles (LUV) according to previously described methods (69). Briefly, they were subjected to 10 freeze/thaw cycles and extruded in a LIPEX Liposome Extrusion System using 0.1-μm pore size Nuclepore filters (Whatman). Liposomes were loaded on a PD10 gel filtration column (GE Healthcare) equilibrated in Calcein Leakage Buffer (10 mM Hepes-KOH, 130 mM NaCl, pH 7.4). Liposome leakage was measured mixing 110 μL liposomes (11 μM) and 10 μL α-syn (10 μM). Leakage controls, 0 and 100%, were obtained adding to the same liposome sample 10 μL of Calcein Leakage Buffer or Triton X-100 10% (vol/vol), respectively. Samples were incubated for 2 h at 25 °C with constant shaking (350 rpm). Fluorescence was measured at 25 °C in a FluoroMax-3 (Jobin-Ybon) fluorimeter using excitation and emission wavelengths of 440 and 520 nm.

MTS Assay. SH-SY5Y cells were seeded at 20,000 cells/well in 96-well plates and incubated overnight in Dulbecco's modified Eagle's medium low glucose with 1 g/L L-glutamine supplemented with 10% heat-inactivated fetal bovine serum, penicillin and streptomycin (50 U/mL and 50 μg/mL, respectively), and MycoZap Prophylactic (Lonza, 1/1,000 dilution). The next day, the medium was replaced by 100 μL of fresh medium containing 0.15 or 0.3 μM of α-syn, and cells were incubated for 24 h. The freshly prepared MTS/PES mixture was directly added (20 μL) to culture wells and incubated for 1 to 4 h. Formazan formation was measured by recording the absorbance at 490 nm in a Synergy HTX plate reader (Biotek). Control values of cells without α-syn and culture medium without cells were taken as 100 and 0% cell viability, respectively.

AFM and HS-AFM Images. Bare mica was covered with 100 μL Poly-L-lysine solution (Sigma, P8920) for 5 min for the AFM (JPK, Nanowizard 3 Ultra-Speed2) images or 10 μL Poly-L-Ornithine (Sigma, P4957) for the HS-AFM (Bruker, NanoRacer) measurements and rinsed three times with Disaggregation Buffer. Fibrils were deposited onto the surface, incubated for 15 min, and gently rinsed three times with 500 μL or 10 μL of disaggregation buffer for the AFM or HS-AFM experiments, respectively. Finally, 1,800/800 μL of this buffer were added to the chambers for AFM/HS-AFM experiments, and after the identification of interesting spots, 100/50 (AFM/HS-AFM) μL of the chaperone mixture were incorporated into the samples. Finally, a solution containing ATP and ATP-RS was added to the imaging chamber, resulting in final sample volumes of 2,000 μL and 900 μL. The AFM equipment was operated in QI mode with MSNL-10 cantilevers (Bruker). For fast imaging with HS-AFM, tapping mode and USC-F1.2 (NanoWorld) cantilevers were used. Images and movies were analyzed with JPKSPM Data Processing, ImageJ, and WSxM software.

Statistical Analysis. All measurements were done at least three times, and levels of significance were determined by a two-tailed Student's t test. A value of $P < 0.05$ was considered statistically significant.

Data Availability. All study data are included in the article and/or supporting information.

1. I. C. Brás, M. Xylaki, T. F. Outeiro, Mechanisms of alpha-synuclein toxicity: An update and outlook. *Prog. Brain Res.* **252**, 91–129 (2020).
2. M. G. Erkkinen, M. O. Kim, M. D. Geschwind, Clinical neurology and epidemiology of the major neurodegenerative diseases. *Cold Spring Harb. Perspect. Biol.* **10**, a033118 (2018).
3. G. M. Halliday, J. L. Holton, T. Revesz, D. W. Dickson, Neuropathology underlying clinical variability in patients with synucleinopathies. *Acta Neuropathol.* **122**, 187–204 (2011).
4. N. Cremades *et al.*, Direct observation of the interconversion of normal and toxic forms of α-synuclein. *Cell* **149**, 1048–1059 (2012).
5. M. Iljina *et al.*, Kinetic model of the aggregation of alpha-synuclein provides insights into prion-like spreading. *Proc. Natl. Acad. Sci. U.S.A.* **113**, E1206–E1215 (2016).
6. X. Li *et al.*, Early stages of aggregation of engineered α-synuclein monomers and oligomers in solution. *Sci. Rep.* **9**, 1734 (2019).
7. P. Alam, L. Bousset, R. Melki, D. E. Otzen, α-synuclein oligomers and fibrils: A spectrum of species, a spectrum of toxicities. *J. Neurochem.* **150**, 522–534 (2019).
8. B. Winner *et al.*, In vivo demonstration that alpha-synuclein oligomers are toxic. *Proc. Natl. Acad. Sci. U.S.A.* **108**, 4194–4199 (2011).
9. R. Sharon *et al.*, The formation of highly soluble oligomers of alpha-synuclein is regulated by fatty acids and enhanced in Parkinson's disease. *Neuron* **37**, 583–595 (2003).
10. K. E. Paleologou *et al.*, Detection of elevated levels of soluble alpha-synuclein oligomers in post-mortem brain extracts from patients with dementia with Lewy bodies. *Brain* **132**, 1093–1101 (2009).

11. N. Cremades, S. W. Chen, C. M. Dobson, Structural characteristics of α-synuclein oligomers. *Int. Rev. Cell Mol. Biol.* **329**, 79–143 (2017).

12. K. M. Danzer *et al.*, Exosomal cell-to-cell transmission of alpha synuclein oligomers. *Mol. Neurodegener.* **7**, 42 (2012).

13. P. Desplats *et al.*, Inclusion formation and neuronal cell death through neuron-to-neuron transmission of alpha-synuclein. *Proc. Natl. Acad. Sci. U.S.A.* **106**, 13010–13015 (2009).

14. J. M. Froula *et al.*, Defining α-synuclein species responsible for Parkinson's disease phenotypes in mice. *J. Biol. Chem.* **294**, 10392–10406 (2019).

15. K. C. Luk *et al.*, Exogenous alpha-synuclein fibrils seed the formation of Lewy body-like intracellular inclusions in cultured cells. *Proc. Natl. Acad. Sci. U.S.A.* **106**, 20051–20056 (2009).

16. L. A. Volpicelli-Daley *et al.*, Exogenous α-synuclein fibrils induce Lewy body pathology leading to synaptic dysfunction and neuron death. *Neuron* **72**, 57–71 (2011).

17. W. Peelaerts *et al.*, α-Synuclein strains cause distinct synucleinopathies after local and systemic administration. *Nature* **522**, 340–344 (2015).

18. N. L. Rey, G. H. Petit, L. Bousset, R. Melki, P. Brundin, Transfer of human α-synuclein from the olfactory bulb to interconnected brain regions in mice. *Acta Neuropathol.* **126**, 555–573 (2013).

19. T. P. Knowles *et al.*, An analytical solution to the kinetics of breakable filament assembly. *Science* **326**, 1533–1537 (2009).

20. A. K. Buell *et al.*, Solution conditions determine the relative importance of nucleation and growth processes in α-synuclein aggregation. *Proc. Natl. Acad. Sci. U.S.A.* **111**, 7671–7676 (2014).

21. J. Labbadia, R. I. Morimoto, The biology of proteostasis in aging and disease. *Annu. Rev. Biochem.* **84**, 435–464 (2015).

22. M. L. Duennwald, A. Echeverria, J. Shorter, Small heat shock proteins potentiate amyloid dissolution by protein disaggregases from yeast and humans. *PLoS Biol.* **10**, e1001346 (2012).

23. X. Gao *et al.*, Human Hsp70 disaggregase reverses Parkinson's-linked α-synuclein amyloid fibrils. *Mol. Cell* **59**, 781–793 (2015).

24. E. Nachman *et al.*, Disassembly of Tau fibrils by the human Hsp70 disaggregation machinery generates small seeding-competent species. *J. Biol. Chem.* **295**, 9676–9690 (2020).

25. A. Scior *et al.*, Complete suppression of Htt fibrilization and disaggregation of Htt fibrils by a trimeric chaperone complex. *EMBO J.* **37**, 282–299 (2018).

26. L. Ferrari *et al.*, Human chaperones untangle fibrils of the Alzheimer protein Tau. *bioRxiv* [Preprint] (2018). https://doi.org/10.1101/426650 (Accessed 20 March 2021).

27. N. Bengoa-Vergniory, R. F. Roberts, R. Wade-Martins, J. Alegre-Abarrategui, Alpha-synuclein oligomers: A new hope. *Acta Neuropathol.* **134**, 819–838 (2017).

28. G. Fusco *et al.*, Structural basis of membrane disruption and cellular toxicity by α-synuclein oligomers. *Science* **358**, 1440–1443 (2017).

29. S. W. Chen *et al.*, Structural characterization of toxic oligomers that are kinetically trapped during α-synuclein fibril formation. *Proc. Natl. Acad. Sci. U.S.A.* **112**, E1994–E2003 (2015).

30. E. Deas *et al.*, Alpha-synuclein oligomers interact with metal ions to induce oxidative stress and neuronal death in Parkinson's disease. *Antioxid. Redox Signal.* **24**, 376–391 (2016).

31. P. R. Angelova *et al.*, Ca2+ is a key factor in α-synuclein-induced neurotoxicity. *J. Cell Sci.* **129**, 1792–1801 (2016).

32. J. D. Camino *et al.*, The extent of protein hydration dictates the preference for heterogeneous or homogeneous nucleation generating either parallel or antiparallel β-sheet α-synuclein aggregates. *Chem. Sci. (Camb.)* **11**, 11902–11914 (2020).

33. D. M. Cyr, C. H. Ramos, Specification of Hsp70 function by Type I and Type II Hsp40. *Subcell. Biochem.* **78**, 91–102 (2015).

34. N. B. Nillegoda *et al.*, Crucial HSP70 co-chaperone complex unlocks metazoan protein disaggregation. *Nature* **524**, 247–251 (2015).

35. J. T. Jarrett, P. T. Lansbury Jr, Amyloid fibril formation requires a chemically discriminating nucleation event: Studies of an amyloidogenic sequence from the bacterial protein OsmB. *Biochemistry* **31**, 12345–12352 (1992).

36. S. I. A. Cohen *et al.*, Proliferation of amyloid-β42 aggregates occurs through a secondary nucleation mechanism. *Proc. Natl. Acad. Sci. U.S.A.* **110**, 9758–9763 (2013).

37. W. F. Xue *et al.*, Fibril fragmentation enhances amyloid cytotoxicity. *J. Biol. Chem.* **284**, 34272–34282 (2009).

38. G. Ghag *et al.*, Soluble tau aggregates, not large fibrils, are the toxic species that display seeding and cross-seeding behavior. *Protein Sci.* **27**, 1901–1909 (2018).

39. H. Mirbaha *et al.*, Inert and seed-competent tau monomers suggest structural origins of aggregation. *eLife* **7**, e36584 (2018).

40. H. Mirbaha, B. B. Holmes, D. W. Sanders, J. Bieschke, M. I. Diamond, Tau trimers are the minimal propagation unit spontaneously internalized to seed intracellular aggregation. *J. Biol. Chem.* **290**, 14893–14903 (2015).

41. H. Abdelmotilib *et al.*, α-Synuclein fibril-induced inclusion spread in rats and mice correlates with dopaminergic Neurodegeneration. *Neurobiol. Dis.* **105**, 84–98 (2017).

42. J. L. Arrondo, A. Muga, J. Castresana, F. M. Goñi, Quantitative studies of the structure of proteins in solution by Fourier-transform infrared spectroscopy. *Prog. Biophys. Mol. Biol.* **59**, 23–56 (1993).

43. P. K. Auluck, G. Caraveo, S. Lindquist, α-Synuclein: Membrane interactions and toxicity in Parkinson's disease. *Annu. Rev. Cell Dev. Biol.* **26**, 211–233 (2010).

44. S. Thirunavukkuarasu, E. A. Jares-Erijman, T. M. Jovin, Multiparametric fluorescence detection of early stages in the amyloid protein aggregation of pyrene-labeled alpha-synuclein. *J. Mol. Biol.* **378**, 1064–1073 (2008).

45. D. L. Floyd, S. C. Harrison, A. M. van Oijen, Analysis of kinetic intermediates in single-particle dwell-time distributions. *Biophys. J.* **99**, 360–366 (2010).

46. J. M. G. Vilar, C. C. Guet, S. Leibler, Modeling network dynamics: The lac operon, a case study. *J. Cell Biol.* **161**, 471–476 (2003).

47. A. Novick, M. Weiner, Enzyme induction as an all-or-none phenomenon. *Proc. Natl. Acad. Sci. U.S.A.* **43**, 553–566 (1957).

48. A. S. Wentink *et al.*, Molecular dissection of amyloid disaggregation by human HSP70. *Nature* **587**, 483–488 (2020).

49. D. R. Boyer *et al.*, Structures of fibrils formed by α-synuclein hereditary disease mutant H50Q reveal new polymorphs. *Nat. Struct. Mol. Biol.* **26**, 1044–1052 (2019).

50. D. R. Boyer *et al.*, The α-synuclein hereditary mutation E46K unlocks a more stable, pathogenic fibril structure. *Proc. Natl. Acad. Sci. U.S.A.* **117**, 3592–3602 (2020).

51. R. Guerrero-Ferreira *et al.*, Two new polymorphic structures of human full-length alpha-synuclein fibrils solved by cryo-electron microscopy. *eLife* **8**, e48907 (2019).

52. R. Guerrero-Ferreira *et al.*, Cryo-EM structure of alpha-synuclein fibrils. *eLife* **7**, e36402 (2018).

53. B. Li *et al.*, Cryo-EM of full-length α-synuclein reveals fibril polymorphs with a common structural kernel. *Nat. Commun.* **9**, 3609 (2018).

54. Y. Li *et al.*, Amyloid fibril structure of α-synuclein determined by cryo-electron microscopy. *Cell Res.* **28**, 897–903 (2018).

55. X. Ni, R. P. McGlinchey, J. Jiang, J. C. Lee, Structural insights into α-synuclein fibril polymorphism: Effects of Parkinson's disease-related C-terminal truncations. *J. Mol. Biol.* **431**, 3913–3919 (2019).

56. M. Schweighauser *et al.*, Structures of α-synuclein filaments from multiple system atrophy. *Nature* **585**, 464–469 (2020).

57. Y. Sun *et al.*, Cryo-EM structure of full-length α-synuclein amyloid fibril with Parkinson's disease familial A53T mutation. *Cell Res.* **30**, 360–362 (2020).

58. Y. V. Taguchi *et al.*, Hsp110 mitigates α-synuclein pathology in vivo. *Proc. Natl. Acad. Sci. U.S.A.* **116**, 24310–24316 (2019).

59. J. Tittelmeier *et al.*, The HSP110/HSP70 disaggregation system generates spreading-competent toxic α-synuclein species. *EMBO J.* **39**, e103954 (2020).

60. E. A. Nollen, J. F. Brunsting, J. Song, H. H. Kampinga, R. I. Morimoto, Bag1 functions in vivo as a negative regulator of Hsp70 chaperone activity. *Mol. Cell. Biol.* **20**, 1083–1088 (2000).

61. B. G. Wilhelm *et al.*, Composition of isolated synaptic boutons reveals the amounts of vesicle trafficking proteins. *Science* **344**, 1023–1028 (2014).

62. A. Finka, P. Goloubinoff, Proteomic data from human cell cultures refine mechanisms of chaperone-mediated protein homeostasis. *Cell Stress Chaperones* **18**, 591–605 (2013).

63. H. J. Lee, S. Patel, S. J. Lee, Intravesicular localization and exocytosis of alpha-synuclein and its aggregates. *J. Neurosci.* **25**, 6016–6024 (2005).

64. P. Nirdé *et al.*, Heat shock cognate 70 protein secretion as a new growth arrest signal for cancer cells. *Oncogene* **29**, 117–127 (2010).

65. P. Gracia, J. D. Camino, L. Volpicelli-Daley, N. Cremades, Multiplicity of α-synuclein aggregated species and their possible roles in disease. *Int. J. Mol. Sci.* **21**, 8043 (2020).

66. Y. Cabrera *et al.*, Regulation of human Hsc70 ATPase and chaperone activities by Apg2: Role of the acidic subdomain. *J. Mol. Biol.* **431**, 444–461 (2019).

67. C. Huang, G. Ren, H. Zhou, C. C. Wang, A new method for purification of recombinant human α-synuclein in *Escherichia coli*. *Protein Expr. Purif.* **42**, 173–177 (2005).

68. S. Barghorn, J. Biernat, E. Mandelkow, Purification of recombinant tau protein and preparation of Alzheimer-paired helical filaments in vitro. *Methods Mol. Biol.* **299**, 35–51 (2005).

69. L. D. Mayer, M. J. Hope, P. R. Cullis, Vesicles of variable sizes produced by a rapid extrusion procedure. *Biochim. Biophys. Acta* **858**, 161–168 (1986).

Franco et al.
All-or-none amyloid disassembly via chaperone-triggered fibril unzipping favors clearance of α-synuclein toxic species

PNAS | 11 of 11
https://doi.org/10.1073/pnas.2105548118

www.manaraa.com